Since January 2020 Elsevier has created a COVID-19 resource centre with free information in English and Mandarin on the novel coronavirus COVID-19. The COVID-19 resource centre is hosted on Elsevier Connect, the company's public news and information website.

Journal of Aerosol Science 173 (2023) 106179

Contents lists available at ScienceDirect

Journal of Aerosol Science

journal homepage: www.elsevier.com/locate/jaerosci

Influence of two-dimensional expiratory airflow variations on respiratory particle propagation during pronunciation of the fricative [f]

Amir A. Mofakham [a,*], Brian T. Helenbrook [a], Byron D. Erath [a], Andrea R. Ferro [b], Tanvir Ahmed [a], Deborah M. Brown [c], Goodarz Ahmadi [a]

[a] Department of Mechanical and Aerospace Engineering, Clarkson University, Potsdam, NY 13699, United States of America
[b] Department of Civil and Environmental Engineering, Clarkson University, Potsdam, NY 13699, United States of America
[c] Joint Educational Programs, Trudeau Institute, Saranac Lake, NY 12983, United States of America

ARTICLE INFO

Editor: Dr. Chris Hogan

Keywords:
Speech
Fricative
Expiratory airflow
Respiratory particles
COVID-19

ABSTRACT

Propagation of respiratory particles, potentially containing viable viruses, plays a significant role in the transmission of respiratory diseases (e.g., COVID-19) from infected people. Particles are produced in the upper respiratory system and exit the mouth during expiratory events such as sneezing, coughing, talking, and singing. The importance of considering speaking and singing as vectors of particle transmission has been recognized by researchers. Recently, in a companion paper, dynamics of expiratory flow during fricative utterances were explored, and significant variations of airflow jet trajectories were reported. This study focuses on respiratory particle propagation during fricative productions and the effect of airflow variations on particle transport and dispersion as a function of particle size. The commercial ANSYS-Fluent computational fluid dynamics (CFD) software was employed to quantify the fluid flow and particle dispersion from a two-dimensional mouth model of sustained fricative [f] utterance as well as a horizontal jet flow model. The fluid velocity field and particle distributions estimated from the mouth model were compared with those of the horizontal jet flow model. The significant effects of the airflow jet trajectory variations on the pattern of particle transport and dispersion during fricative utterances were studied. Distinct differences between the estimations of the horizontal jet model for particle propagation with those of the mouth model were observed. The importance of considering the vocal tract geometry and the failure of a horizontal jet model to properly estimate the expiratory airflow and respiratory particle propagation during the production of fricative utterances were emphasized.

1. Introduction

The transmission of viral expiratory particles and aerosols emitted from infected individuals has been recognized as one of the primary modes of transmission of the COVID-19 virus from one person to another (Jayaweera, Perera, Gunawardana, & Manatunge, 2020). The devastating epidemics caused by viral respiratory diseases (e.g., COVID-19, MERS-CoV, Measles, influenza) highlight the need to advance knowledge regarding the spread of particles expirated during human expiratory activities to plan an effective response to reduce infection.

* Corresponding author.
E-mail address: amir.mofakham@gmail.com (A.A. Mofakham).

https://doi.org/10.1016/j.jaerosci.2023.106179
Received 18 February 2022; Received in revised form 19 February 2023; Accepted 27 March 2023
Available online 11 April 2023

Nomenclature

C_c	Stokes–Cunningham slip correction factor
C_D	Particle drag coefficient
d_p	Particle diameter
dt	Time step
$\vec{g}$	Acceleration of gravity
$\vec{G}(t)$	Vector Gaussian random number with zero mean and unit variance
h	Tooth gap height
$\hat{j}$	The standard unit direction in the y-direction
k_b	Boltzmann constant
m_p	Particle mass
$\vec{n}(t)$	Brownian force per unit mass
N_t	Total number of instances
N_{pt}	Total number of particle counts in all bins during the whole expiration at 0.50 s
p	Static pressure
p_s	Subglottal pressure
Re_p	Particle Reynolds number
S	Particle to fluid density ratio
S_0	Spectral density of Gaussian
t	Time
T	Absolute temperature
$\vec{v}$	Fluid velocity
$\vec{v}_p$	Particle velocity
λ	Gas molecular mean free path
μ	Fluid dynamic viscosity
ρ	Fluid density
ρ_p	Particle density
$\bar{\bar{\tau}}$	Stress tensor
τ_p	Particle relaxation time
ν	Fluid kinematic viscosity

Respiratory particles are generated during breathing, speaking, singing, sneezing, and coughing. Until recently, the role of speaking in generating and transmitting respiratory particles was largely neglected, as coughing and sneezing were deemed more dominant (Stadnytskyi, Bax, Bax, & Anfinrud, 2020). However, recent investigations affirmed that the aerosol generation by speech is comparable to that of coughing (Asadi et al., 2020; Johnson et al., 2011; Lindsley et al., 2012; Yan et al., 2018). In addition, the size distribution of speech particles is relatively similar to those of coughing and singing (Chao et al., 2009; Duguid, 1946; Johnson et al., 2011). Therefore, it is essential to assess the risk of speech generated respiratory particles to be incorporated in guidelines and recommendations provided for respiratory pandemics.

To quantify the risk of particle propagation during speech, it is required to know the airflow velocity field expired during speech. Accordingly, in companion papers, physical (Ahmed et al., 2021) and numerical (Mofakham et al., 2022) experiments were performed to evaluate the distributions of airflow fluid velocity trajectories expelled during sustained consonant fricative productions and the influence of the speech loudness and changes in vocal tract geometry on the airflow dynamics. In these studies the unsteady nature of the flow was measured and simulated. Both studies showed significant unsteadiness in the magnitude and direction of the flow velocity. The flow simulations were 2D while the experiments were 3D, but both led to the conclusion that the flow direction is highly unsteady and time-varying. However, the propagation of respiratory particles has not been directly assessed.

Aside from a few exceptions (Abkarian, Mendez, Xue, Yang, & Stone, 2020), the unsteady behavior of expiratory flow is typically overlooked in most studies (Liu, Qian, Luo, & Zheng, 2021; Singhal, Ravichandran, Govindarajan, & Diwan, 2021; Yang, Pahlavan, Mendez, Abkarian, & Stone, 2020), and a steady, horizontal jet exiting from a simplified vocal tract geometry is employed to estimate expiratory airflow and respiratory particle propagation during expiratory activities.

Because the significance of unsteady and dynamic expiratory airflow trajectories on particle transport during speech has not been fully investigated, this investigation is devoted to identifying how the previously identified unsteady expiratory airflow dynamics influence particle propagation. In addition, the validity of the simplified horizontal jet flow approach will also be explored. This is an important distinction as running speech produces a wide range of phonemes that are anticipated to lead to complex and variable behavior. Fricatives, which are produced by an airflow restriction in the mouth, produce the highest airflow velocity, with complex dynamics (Pont, Guasch, Baiges, Codina, & Van Hirtum, 2019; Yoshinaga, Nozaki, & Wada, 2019). Among different fricatives, the

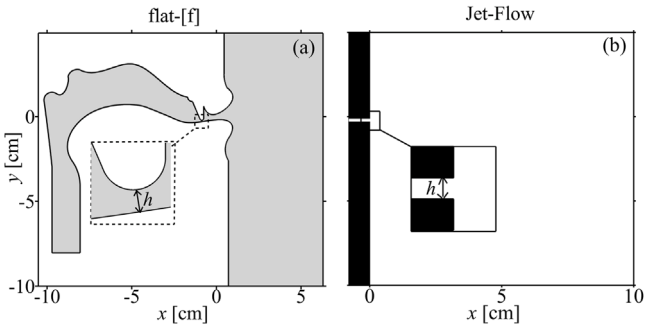

Fig. 1. (a) Silhouette of the vocal tract geometry of fricative [f] utterance. The inset shows a zoomed-in view of the mouth geometry, with the wall-normal gap between the lower lip and the upper tooth defined as h. (b) The geometry of the horizontal jet model with a vertical opening. The inset shows a zoomed-in view of the opening with a height equal to the tooth gap (h).

fricative utterance [f] produced by a labiodental occlusion was chosen to be explored in this investigation, because it is representative of the upper limit on the airflow velocity and volumetric flow rate at the mouth that is produced during speech (Wang & Li, 2019). Other fricatives that arise from occlusions at different locations in the vocal tract (e.g., palatal fricative [s]) are likely to create different flow dynamics due to the altered mouth and lip geometry. Accordingly, propagation of expiratory particles during the production of [f] was simulated using a two-dimensional realistic vocal tract model. Results are contrasted with a two-dimensional horizontal jet flow model. The airflow simulations were conducted by direct numerical simulation of the full 2D Navier–Stokes and continuity equations (with no need to use a turbulence model). It is acknowledged that discrepancies may exist between the two-dimensional simulation results reported in this investigation and the actual three-dimensional flow fields (Anderson, Green, & Fels, 2009). However, two-dimensional simulation results are still valid to highlight the influence of the vocal tract geometry on the expiratory flow and the effects of the airflow jet trajectory variations on the propagation of respiratory particles as well as the differences between predictions of a horizontal jet flow and a mouth model.

2. Methods

2.1. Model geometries

Fig. 1.a displays a two-dimensional generalized vocal tract geometry during a sustained fricative [f] production. It was drawn to represent magnetic resonance imaging (MRI) data from a speech dataset of multiple subjects obtained at the mid-sagittal plane of the upper respiratory system of speakers (Mofakham et al., 2022; Narayanan et al., 2014). The representation captures the primary features occurring during the fricative [f] production, including the positioning of the tongue relative to the teeth and the gap between them. The most important feature from a flow perspective is the labiodental constriction created by positioning the lower lip against the upper teeth during [f] utterance. This is shown in the inset of Fig. 1.a.

To produce an average cross-sectional area of 0.20 cm^2 at the constriction (Narayanan, Alwan, & Haker, 1995), a height of 0.8 mm for the minimum gap size between the lower lip and upper tooth was implemented (Mofakham et al., 2022). The Reynolds number at the constriction was around 1700 based on the gap height and the maximum velocity. To find the optimum grid size of the mouth model, four different grids with maximum cell sizes of 40, 20, 10, and 5 μm at the constriction region were generated. The velocity profiles at the constriction region produced by the different computational grids were compared and it was found that the results of the computational grid with 10 μm was approximately identical to those at 5 μm. Therefore, the computational grid with a maximum cell size of 10 μm at the constriction was picked as the optimum grid.

Fig. 1.b shows the geometry of the horizontal jet model, which is a simplified version of the mouth model where the vocal tract geometry was omitted and only a vertical opening with a size equal to the tooth gap height (h = 0.8 mm) of the mouth model was assumed as shown in the inset of Fig. 1.b. In this model, a horizontal airflow jet exits from the vertical opening and spreads into the computational domain. The computational grid of the horizontal jet model was generated with a structure and resolution similar to that of the mouth model to keep the level of accuracy the same between the models.

2.2. Numerical procedure

2.2.1. Flow simulation

To quantify the unsteady expiratory flow field of the two-dimensional mouth model for [f] and the two-dimensional horizontal jet flow, the unsteady viscous flow model of the ANSYS-Fluent CFD software was used to solve the two-dimensional continuity and the Navier–Stokes equations given as

$$\nabla \cdot \vec{v} = 0, \tag{1}$$

$$\frac{\partial}{\partial t}(\rho\vec{v}) + \nabla\cdot(\rho\vec{v}\otimes\vec{v}) = -\vec{\nabla}p + \mu\nabla^2\vec{v} + \rho\vec{g}, \tag{2}$$

where t, $\vec{v}$, ρ, μ, p, and $\vec{g}$ are the time, the fluid velocity, fluid density, fluid dynamic viscosity, fluid static pressure, and acceleration of gravity, respectively.

The simulations were performed with a time step of 10 μs for a duration of 0.50 s starting from a quiescent state, selected based on the mean fricative duration reported in the literature (Lass, 2012; Oller, 1973), while the residual criterion of the continuity, x and y components of the Navier–Stokes equations was set to 10^{-5}. A pressure inlet boundary condition was used to impose a constant pressure of 600 Pa (Titze & Martin, 1998) at the vocal tract inlet section, located below the opening between the vocal folds (glottis), which is representative of the driving pressure produced during speech at normal loudness. From the simulation results an average velocity magnitude of 28.2 m/s was computed at the constriction region between the tooth and the lower lip. Therefore, for the jet model, an inlet velocity boundary condition with a horizontal velocity of 28.2 m/s was assumed for the inlet.

Additional information on the vocal tract geometry, the grid size, more details on the numerical procedure, and the verification and validation of the numerical approach may be found in a companion paper on the airflow dynamics during fricative utterances (Mofakham et al., 2022).

2.2.2. Lagrangian particle tracking

The discrete phase model (DPM) of the ANSYS-Fluent software, where particles were assumed as point particles, was used to quantify the trajectories of 0.1, 1, 5, 10, 20, and 50 μm particles with a density of 1030 kg/m^3 (Johnson et al., 2011; Leal, Smyth, & Ghosh, 2017). The particles were introduced with an injection rate of 5×10^5 particles/s from the tooth gap region of the mouth model and the jet model inlet. By the end of the simulations, at 0.50 s, 25×10^4 particles of a given size were emitted in the computational domain of both models. The trap particle boundary condition was imposed on the vocal tract boundary of the mouth model, and the escape boundary condition was assumed for the boundaries of the external flow domain of both mouth and jet models. It was assumed that the volume fraction of particles was sufficiently small so that the interactions between particles as well as the influence of particles on the flow field were ignored and the simulations were performed under the one-way coupling assumption. The velocity of the particles at each time step was evaluated by the particle equation of motion, including the drag, gravity, and Brownian forces, given as

$$\frac{d\vec{v}_p}{dt} = \frac{1}{\tau_p}\frac{C_D Re_p}{24}(\vec{v}-\vec{v}_p) + \vec{g} + \vec{n}(t), \tag{3}$$

where $\vec{v}_p$ is the particle velocity, $\vec{g}$, the acceleration of gravity is equal to $-9.81\ \hat{j}$ [m/s^2], and $\vec{n}(t)$ is the Brownian force per unit mass, (Li & Ahmadi, 1993) given by

$$\vec{n}(t) = \vec{G}(t)\left(\frac{\pi S_0}{dt}\right)^{0.5}. \tag{4}$$

Here S_0 is given by

$$S_0 = \frac{2k_bT}{\tau_p\pi m_p}, \tag{5}$$

where k_b is the Boltzmann constant equal to 1.38×10^{-23} J/K. In Eq. (3), Re_p is the particle Reynolds number given by

$$Re_p \equiv \frac{\rho d_p|\vec{v}_p-\vec{v}|}{\mu}, \tag{6}$$

and, τ_p is the particle relaxation time defined by

$$\tau_p = \frac{Sd_p^2C_c}{18\nu}, \tag{7}$$

where d_p is the particle diameter and C_c is the Cunningham slip correction factor given as

$$C_c = 1 + \frac{2\lambda}{d_p}(1.257 + 0.4e^{-(1.1d_p/2\lambda)}). \tag{8}$$

Here the gas mean free path, λ, was assumed 0.07 μm for air at room temperature. In Eq. (3), the drag coefficient (C_D) for particles larger than one micron is estimated by the drag model proposed for smooth spherical particles by Morsi and Alexander (1972) given as

$$C_D = a_1 + \frac{a_2}{Re_p} + \frac{a_3}{Re_p^2}, \tag{9}$$

where coefficients a_i are constant defined over different ranges of Re_p. However, assuming the Stokes regime (Ounis, Ahmadi, & McLaughlin, 1991), the drag coefficient of submicron particles is defined by

$$C_D = \frac{24}{Re_p}. \tag{10}$$

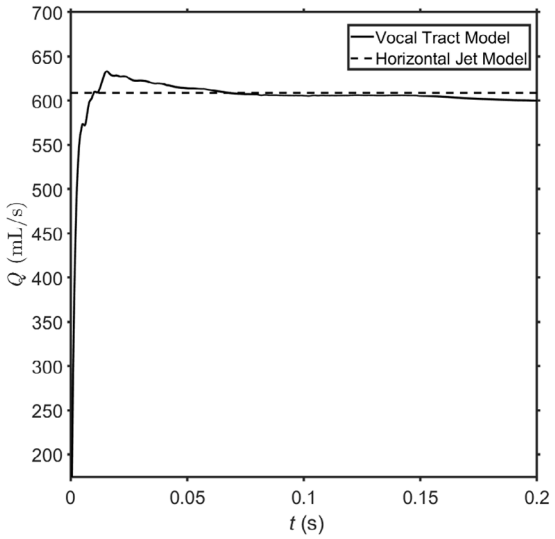

Fig. 2. Time variation of the volumetric flow rate of the mouth and horizontal jet model.

3. Results and discussion

3.1. Expiratory flow field

Fig. 2 displays the time variation of the volumetric flow rate of the mouth model for the utterance [f] and the horizontal jet model. In less than 0.05 s, the mouth model reaches its quasi-steady value of about 600 mL/s, which is about 2–4 times greater than the usual flow rate in speech. The quasi-steady value of the mouth model matches the steady flow rate of the horizontal jet model. Video A in the supplementary shows the fluid velocity contours of the mouth and the horizontal jet model versus time. Although Fig. 2 shows the volumetric flow rates appear to stabilize, Video A reveals the flow at the exit of the mouth, and the horizontal jet model is highly unstable. The direction of airflow changes rapidly, causing significant fluctuations in fluid propagation. The unsteadiness is particularly more pronounced in the mouth model, producing noticeable differences compared to the fluid flow in the horizontal jet model.

By exploring the expiratory fluid velocities it is revealed that during fricative [f] productions, an airflow jet is produced at the constriction that exits into the surroundings from the space between lips. As a result of the Coandă effect (Coanda, 1936), the jet tends to attach to either the upper or lower lip producing expiratory flow that is propagated with positive or negative angles relative to the horizontal. As noted before, the jet is unstable and small variations in volume flow rate (i.e., loudness), shape of the vocal tract, or interactions with the vortical flow structures cause the jet to oscillate between the lips (Ahmed et al., 2021; Mofakham et al., 2022).

To clarify the evolution of the airflow jet trajectories over the 0.50 s of the [f] production, the instantaneous angle of the airflow jet was determined by finding the angle of a linear line anchored to the middle of the tooth opening and fitted to the locations of the maximum instantaneous fluid velocity over 0 to 3 cm from the tooth as illustrated in Fig. 3.

The variation of the jet angle versus time is plotted in Fig. 4.a which illustrates that the jet trajectory angles span approximately between $\pm 75°$. As seen from this figure, initially the jet is attached to the upper lip, propagating predominately in the positive direction, but at approximately 0.19 s, the jet migrates towards the lower lip, producing trajectories with more negative orientations. The bimodal distribution of jet angles is also noticeable in Fig. 4.b, where the normalized number of occurrences of jet trajectories with angles distributed in bins with a width of 5° is illustrated. Upward oriented trajectories are distributed around $+35°$ and downward oriented trajectories are distributed around $-15°$, while the mean value is almost horizontal with an angle of $+1.61°$. The abrupt changes in the jet angle are due to far-field disturbance interacting with the near-field jet, similarly observed in the physical measurements (Ahmed et al., 2021). As seen in supplementary Video A, on some occasions, far-field vortical structures cause disruptions at the mouth and jet exit leading to abrupt changes in the estimated jet angles. These occurrences show that in real work scenarios, external flow disturbances may cause even greater variability in the flow direction. The corresponding time history and histogram distributions of the airflow jet trajectory angle expelled from the horizontal jet model are illustrated in Fig. 4c and d, respectively. Fig. 4c indicates the airflow jet trajectories produced by the jet model are predominately horizontal, but as a result of vortices that are shed and spread earlier into the surrounding, they oscillate roughly between $\pm 40°$ with a mean value of $-1.33°$. Fig. 4.d displays a narrow unimodal distribution for the jet angle variations ranging from $-40°$ to $+40°$ with the maximum value in the horizontal direction (e.g., 0°).

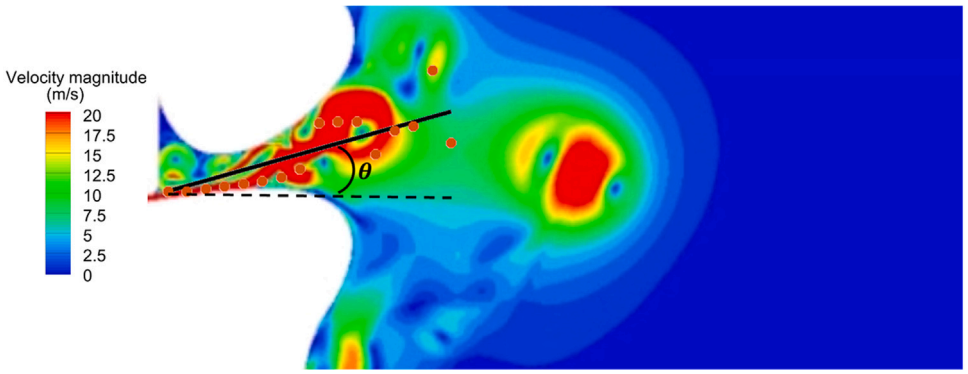

Fig. 3. An example of how the jet angle was computed at the mouth exit, where the dashed line represents the horizontal, and the solid line shows the best-fitted line to the locations of the maximum instantaneous fluid velocity over 0 to 3 cm from the tooth.

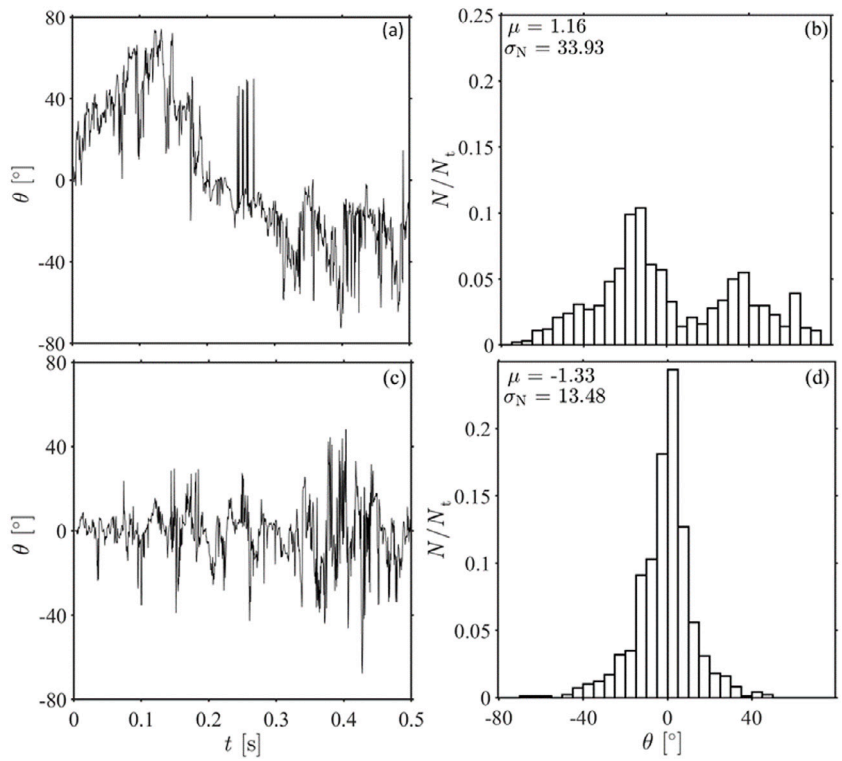

Fig. 4. The time history of angle variations of airflow jet trajectory spreading from (a) the mouth and (c) the horizontal jet model, over the simulation time of 0.50 s. Histograms of the airflow jet trajectory angle distributions normalized by the total number of occurrences are also shown for (b) the mouth and (d) the horizontal jet model.

3.2. Respiratory particle propagation

The evolution of the trajectory of particles with diameters of 0.1, 1, 5, 10, 20, and 50 μm were evaluated during 0.50 s of sustained fricative production in the mouth and jet models. The particles were continuously injected throughout the 0.50 s simulation time.

Video B in the supplementary material presents the propagation of 0.1, 1, 20, and 50 μm particles through the horizontal jet and mouth models. A snapshot of distributions of 0.1, 1, 20, and 50 μm particles from the mouth model at 0.25 and 0.50 s are also illustrated in Fig. 5.a and b, respectively. The corresponding instantaneous airflow velocity contours at 0.25 and 0.50 s are illustrated in Fig. 5.c and d, respectively, where for better visualization, the velocity contours larger than 10 m/s are shown by the red color. To clarify the details at the mouth exit a zoomed in view of the region near the mouth exit is shown in the figures. In Video B and Fig. 5.a and b, the distributions of 0.1 and 1 μm particles are almost identical. This reveals that the Brownian excitation for 0.1 μm particles are small resulting in negligible differences in the trajectories. Comparing the distributions of 0.1 and 1 μm particles,

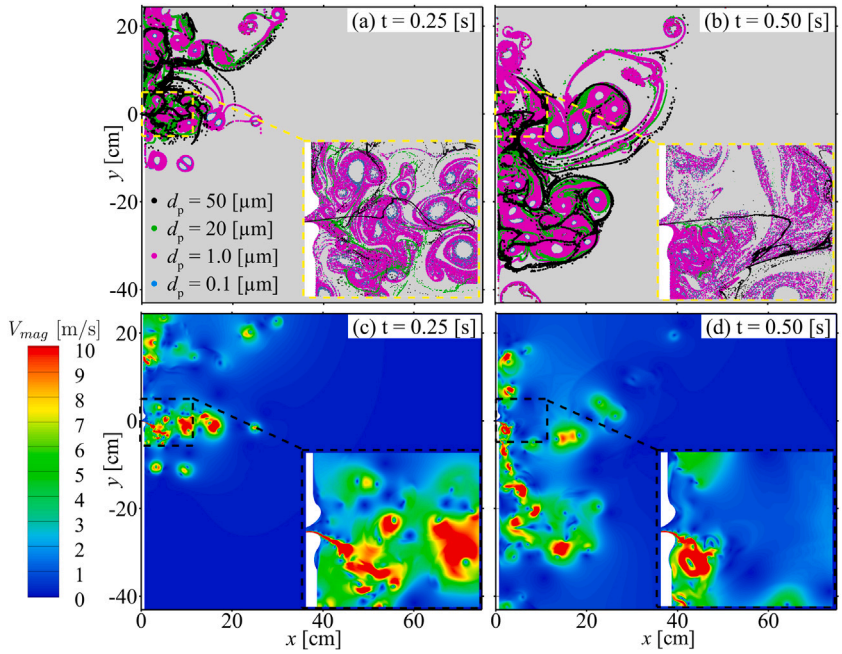

Fig. 5. The instantaneous velocity contours at (a) 0.25 and (b) 0.50 s and a snapshot of distribution of particles with diameters of 0.1, 1, 20, and 50 μm at (c) 0.25 and (d) 0.50 s propagated from the mouth model. The insets show a zoomed in view near the mouth exit.

shown in Fig. 5.a and b, with the airflow velocity contours, shown in Fig. 5.c and d, confirms that these particles follow the flow and end up in the same locations as the vortex cores that shed from the exiting jet. However, for larger particles, due to the increased relaxation times (response time), the tendency of the particles to follow the airflow trajectories reduces. Consequently, as seen in Video B and illustrated in Fig. 5, larger particles (e.g., 20 and 50 μm) only follow the larger vortical structures. The insets in 5.a and b clearly show a ballistic motion of 50 μm particles.

In addition, Fig. 5 shows larger particles accumulate in the outer regions of the vortices, which highlights the influence of the centrifugal force on larger particles. Distributions of the 50 μm particles are roughly similar to those of 20 μm except that, as a result of their larger inertia, they are less dispersed. The influence of the centrifugal force is more pronounced for 50 μm such that they are aggregated at a greater distance from the center of the vortices. The number of injected particles is the same for all sizes, and after 0.50 s of emission, 250,000 particles of each size are introduced into the domain.

The particle distributions of 0.1, 1, 20, and 50 μm resulting from the horizontal jet model at 0.25 and 0.50 s are illustrated in Fig. 6.a and b, respectively. The associated instantaneous airflow velocity contours are shown in Fig. 6.c and d, respectively, where the red color contours represent velocities larger than 10 m/s. Similar to what was seen in the mouth model (Fig. 5), in the horizontal jet model (Fig. 6), the smaller particles (0.1 and 1 μm) follow both small and large size airflow vortices, but the larger particles (20 and 50 μm) are mainly carried by the larger vortical structures. The comparison of Fig. 6.c and d with Fig. 5.c and d, also clarifies that the airflow trajectories produced by the horizontal jet are remarkably different than the mouth trajectories resulting in significant different particle transmission patterns. Fig. 5.a illustrates that particles for the mouth model propagate to higher heights relative to the mouth outlet and spread to the upper boundary of the computational domain at $y = 24.4$ cm. This is due to the positive angle of the airflow jet trajectories during the initial 0.19 s of expiration, as discussed in Section 3.1. However, from 0.25 to 0.50 s, migration of the jet towards the lower lip produces increasingly negative airflow jet trajectories and subsequently lower particle trajectories. In addition, particles that were ejected upward during the initial 0.25 s are also advected towards the lower heights in the computational domain during this time. Consequently, at 0.50 s particles spread downward to $y = -35$ cm relative to the mouth outlet as seen in Fig. 5.b. In contrast, Fig. 6.a reveals that at 0.25s, particles expelled by the horizontal jet are spread symmetrically spanning approximately between ±15 cm in the y-direction. At 0.50 s, shown in Fig. 6.b, the horizontal jet produces particle distributions ranging from −15 and +24 cm in the y-direction, while a random vortex structure carries some particles to regions as low as −40 cm below the mouth exit. Fig. 5.a and b reveal particles are propagated in the horizontal direction up to 30 and 50 cm away from the mouth exit at 0.25 and 0.50 s of expiration, respectively. In contrast, the horizontal jet model propagates particles 40 and 70 cm, as shown in Fig. 6.a and d, respectively.

Because particles are strongly influenced by the high-velocity airflow structures, and the relatively short simulation time of 0.50 s, the influence of gravity on the large particles (e.g., 50 μm) is not observed in Figs. 5 and 6.

Snapshots of particle distribution display only instantaneous particle positions evolving in time as a result of their interactions with vortices and velocity fluctuations. To gain a sense of the particle concentration at any location, the cumulative particle

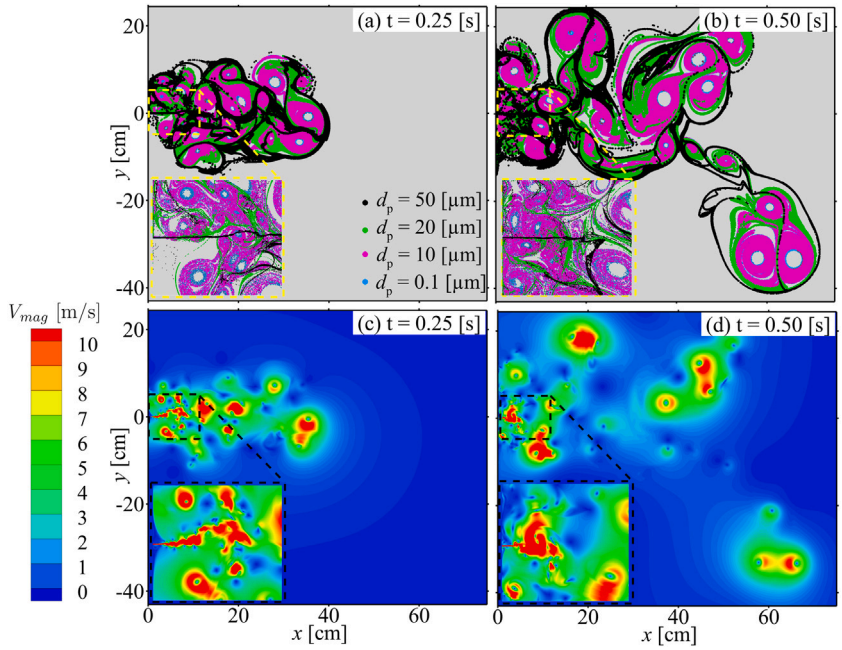

Fig. 6. The instantaneous velocity contours at (a) 0.25 and (b) 0.50 s and a snapshot of distribution of particles with diameters of 0.1, 1, 20, and 50 μm at (c) 0.25 and (d) 0.50 s propagated from the horizontal jet model.

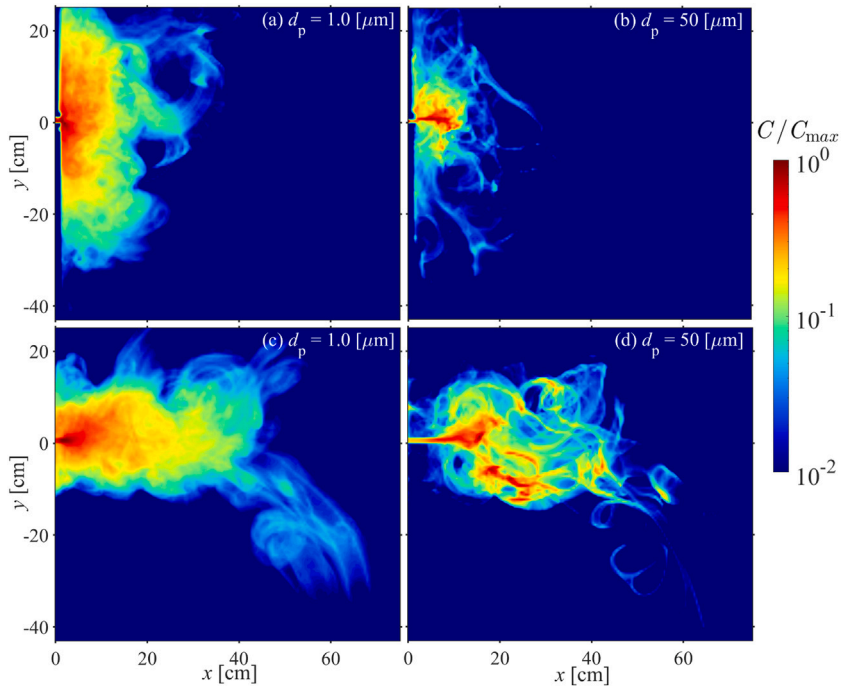

Fig. 7. The contours of cumulative normalized concentration of particles with diameters of 1 and 50 μm at 0.50 s emitted from the (a)–(b) mouth and (c)–(d) jet models in a duration of 0.50 s expiratory flow.

concentrations throughout the 0.50 s of expiration normalized by the maximum cumulative concentration is shown in Fig. 7.a and b for 1 and 50 μm particles at 0.50 s emitted from the mouth model.

Fig. 7.a presents the cumulative 1 μm particle concentrations at 0.50 s for the mouth model, showing they spread over 30 cm in the x-direction. Due to the time variation of the expiratory airflow trajectories, particles also spread between +25 cm to −35 cm in

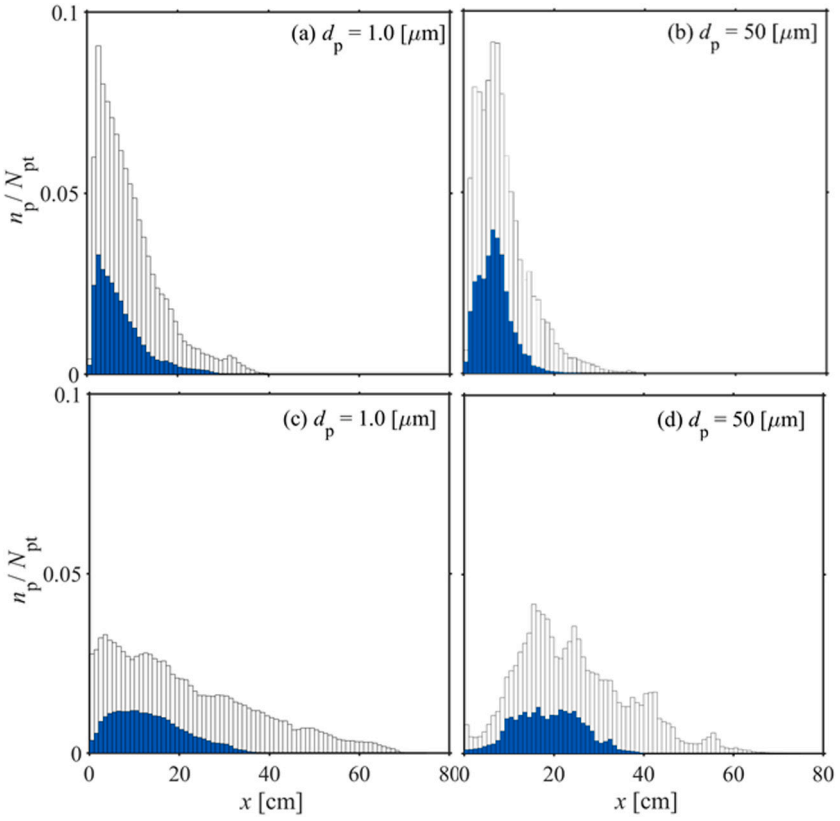

Fig. 8. The normalized histogram of cumulative number count as a function of particle horizontal position with diameters of 1 and 50 μm emitted from the (a)–(b) mouth and (c)–(d) horizontal jet models during 0.25 s (filled bars) and 0.50 s (unfilled bars) of expiratory flow.

the y-direction. However, Fig. 7.b shows that the 50 μm particles are emitted from the mouth model with a ballistic-like trajectory as a result of the high velocity at the tooth gap region from where they are expelled. The ballistic-like motion of 50 μm particles at the mouth exit is also seen in insets of Fig. 5.c and d. The 50 μm particles spread in the vertical direction only by large-scale vortical flow structures so that small concentrations are seen beyond ±10 cm in the y-direction.

The corresponding cumulative normalized concentration contours of 1 and 50 μm particles propagated from the horizontal jet are presented in Fig. 7.c and d, respectively. Fig. 7.c illustrates a roughly symmetric concentration distribution for 1 μm particles emitted by the horizontal jet model. This figure shows particles are predominately propagated up to 45 cm in the x-direction and between ±15 cm in the y-direction. On the other hand, Fig. 7.d shows the 50 μm particles are emitted from the jet primarily in the horizontal direction and penetrate up to approximately 18 cm, before losing their initial momentum. Thereafter, as a result of large vortical structures in the flow, they are distributed up to approximately 47 cm and ±13 cm in the x- and y-directions, respectively.

The comparison between Fig. 7.a and c as well as Fig. 7.b and d identify significant differences between the mouth model and the jet model. Fig. 7 clarifies that the horizontal jet model predicts larger and smaller particle penetrations in the x- and y-directions, respectively, compared to the mouth estimations. The wide variations in the airflow trajectories expired from the mouth model, shown in Fig. 4.a, cause broader spreading of particles in the y-direction leading to smaller penetration in the x-direction. In contrast, the airflow trajectory produced by the jet model, shown in Fig. 4.b, is predominately horizontal producing a stationary horizontal jet flow that leads to increased horizontal penetration and reduced vertical spreading of the particles.

To further clarify the differences between the predictions of the mouth model with those of the jet model, particles are counted in bins with a width of 0.5 cm during 0.50 s of expiration and normalized by N_{pt}, which is the total number of counts in all bins during the whole expiration at 0.50 s. The time evolution of normalized histograms of cumulative number count as a function of particle horizontal position are evaluated at times t = 0.25 s and 0.50 s. Fig. 8.a and b illustrate the histograms of 1 and 50 μm particles obtained from the mouth model. Fig. 8.c and d show the corresponding histograms of 1 and 50 μm particles evaluated by the jet model. The histograms shown in Fig. 8 present the particle distributions at 0.25 s (filled bars) and at 0.50 s (unfilled bars).

Fig. 8.a and b show that over the 0.50 s of simulation the particles emitted from the mouth model penetrate less than 40 cm from the mouth exit. The center of mass values of histograms Fig. 8.a and b are at 9.65 and 8.64 cm, respectively. Fig. 8.c and d, show that the particles propagated by the horizontal jet flow model are propagated over a larger distance, up to approximately 70 cm. Based on the center of mass of the histograms shown in Fig. 8.c and d, the average horizontal penetration is 21.3 and 24.5 cm for the 1 and 50 μm particles emitted from the jet model, respectively. Fig. 8.a and c show that the highest concentration of 1 μm

particles in the mouth and jet flow models occur at about 2.5 and 3.5 cm, respectively. However, the highest concentration of 50 μm particles in the mouth and jet models are approximately at 6.5 and 15.5 cm as shown in Fig. 8.b and d, respectively.

Fig. 8 confirms that particles appear more frequently at larger distances in the expiratory jet flow model compared to the particles propagated by the mouth model. The difference between the jet trajectory angle variations of the mouth expiratory flow with those of the horizontal jet flow model, shown in Fig. 4, leads to the differences between the horizontal penetration distance of particles. Fig. 4.b shows that the jet model produces predominately stationary horizontal airflow trajectories leading to increased horizontal penetration and reduced vertical spreading of the particles. However, it is known from prior works (Abkarian et al., 2020; Ahmed et al., 2021; Han et al., 2021; Liu et al., 2021; Singhal et al., 2021; Yang et al., 2020) that the general flow behavior at the mouth exit during speaking is highly transient with variable airflow jet trajectories. Therefore, it is concluded that a jet model producing predominately horizontal airflow trajectories is probably not a good representation of the flow and particle transport dynamics.

3.3. Limitations

There are some limitations associated with this study. Namely, two-dimensional simulations were conducted, which are a simplification of the three-dimensional human vocal tract geometry. A flat wall was assumed on the side where the exit of the mouth was positioned instead of a human face and neck geometry. This definitely affects the far-field behavior of the flow, however, the point of this study was to investigate the effect of flow unsteadiness on penetration distance which is primarily determined by the flow in the vicinity of the lips. In addition, the dynamic articulation of the oral cavity, teeth, and lips were neglected and the influences of particles on the airflow and the interactions between particles were ignored which adds some inaccuracies for larger size particles (e.g., 20 and 50 μm). However, the focus of this work was to specifically investigate how variability in the expiratory jet trajectory influences the propagation of respiratory particles. Expiratory jet variability is a key behavior observed in clinical measures of expiratory flows (Ahmed et al., 2021) that is captured by two-dimensional models (Mofakham et al., 2022). As such, despite their geometric simplification, 2D models accurately capture the flow dynamics of interest. However, the current study only explored one fricative utterance ([f]), which was chosen based on the high exit velocity and flow rate observed for this oral posture. As such, it serves as a limiting case. Nevertheless, prior work (Ahmed et al., 2021) has identified that different fricative utterances can produce drastically varying flow trajectories. Therefore, the results presented herein should not be generalized for all consonant or fricative utterances. This also highlights the need for ongoing studies that consider the dynamic nature of the expiratory jet that occurs during running speech.

4. Conclusions

The dispersion and penetration of respiratory particles generated by the expiratory flow during a 0.50 s sustained fricative utterance were investigated using a two-dimensional mouth and horizontal jet model.

Exploring the airflow expired from the mouth model highlighted the significant influence of the Coandă effect on the expired airflow direction leading to wide variations of jet trajectory angle spanning between ±75° in the mouth model. In contrast, the jet model produced trajectories that were largely horizontal, with significantly less spreading in the vertical direction. These differences highlight the importance of the exit boundary conditions (e.g., the lips) in accurately capturing the flow dynamics.

The comparison of large and small respiratory particle distributions revealed drastic differences between the mouth and jet model predictions. The horizontal jet model predicts significantly higher particle penetration in the horizontal direction and less dispersion in the vertical direction in comparison to that of the mouth model.

The failure of the horizontal jet model to accurately estimate respiratory particle propagation during fricative utterance productions showed the remarkable influence of the jet trajectory angle variations of the mouth model on the dispersion and penetration of respiratory particle and the need for including the vocal tract geometry in expiratory air and respiratory particle simulations.

Declaration of competing interest

The authors declare that they have no known competing financial interests or personal relationships that could have appeared to influence the work reported in this paper.

Data availability

Data will be made available on request

Acknowledgments

This work was supported by the National Science Foundation, United States under grant number CBET:2029548. Some of the numerical simulations were conducted on the ACRES cluster which was funded by the National Science Foundation, United States under Grant No. 1925596. We would like to thank the NSF and Clarkson University's Office of Information Technology for providing computational resources and support that contributed to these research results.

Appendix A. Supplementary data

Supplementary material related to this article can be found online at https://doi.org/10.1016/j.jaerosci.2023.106179.

References

Abkarian, M., Mendez, S., Xue, N., Yang, F., & Stone, H. A. (2020). Speech can produce jet-like transport relevant to asymptomatic spreading of virus. *Proceedings of the National Academy of Sciences*, *117*(41), 25237–25245.

Ahmed, T., Wendling, H. E., Mofakham, A. A., Ahmadi, G., Helenbrook, B. T., Ferro, A. R., et al. (2021). Variability in expiratory trajectory angles during consonant production by one human subject and from a physical mouth model: Application to respiratory droplet emission. *Indoor Air*, *31*(6), 1896–1912.

Anderson, P., Green, S., & Fels, S. (2009). Modeling fluid flow in the airway using CFD with a focus on fricative acoustics. In *Proc. 1st* (pp. 146–154).

Asadi, S., Wexler, A. S., Cappa, C. D., Barreda, S., Bouvier, N. M., & Ristenpart, W. D. (2020). Effect of voicing and articulation manner on aerosol particle emission during human speech. *PLoS One*, *15*(1), Article e0227699.

Chao, C. Y. H., Wan, M. P., Morawska, L., Johnson, G. R., Ristovski, Z., Hargreaves, M., et al. (2009). Characterization of expiration air jets and droplet size distributions immediately at the mouth opening. *Journal of Aerosol Science*, *40*(2), 122–133.

Coanda, H. (1936). Device for deflecting a stream of elastic fluid projected into an elastic fluid. US Patent 2, 052, 869.

Duguid, J. (1946). The size and the duration of air-carriage of respiratory droplets and droplet-nuclei. *Epidemiology & Infection*, *44*(6), 471–479.

Han, M., Ooka, R., Kikumoto, H., Oh, W., Bu, Y., & Hu, S. (2021). Experimental measurements of airflow features and velocity distribution exhaled from sneeze and speech using particle image velocimetry. *Building and Environment*, *205*, Article 108293.

Jayaweera, M., Perera, H., Gunawardana, B., & Manatunge, J. (2020). Transmission of COVID-19 virus by droplets and aerosols: A critical review on the unresolved dichotomy. *Environmental Research*, Article 109819.

Johnson, G., Morawska, L., Ristovski, Z., Hargreaves, M., Mengersen, K., Chao, C. Y. H., et al. (2011). Modality of human expired aerosol size distributions. *Journal of Aerosol Science*, *42*(12), 839–851.

Lass, N. (2012). *Contemporary issues in experimental phonetics*. Elsevier.

Leal, J., Smyth, H. D., & Ghosh, D. (2017). Physicochemical properties of mucus and their impact on transmucosal drug delivery. *International Journal of Pharmaceutics*, *532*(1), 555–572.

Li, A., & Ahmadi, G. (1993). Deposition of aerosols on surfaces in a turbulent channel flow. *International Journal of Engineering Science*, *31*(3), 435–451.

Lindsley, W. G., Pearce, T. A., Hudnall, J. B., Davis, K. A., Davis, S. M., Fisher, M. A., et al. (2012). Quantity and size distribution of cough-generated aerosol particles produced by influenza patients during and after illness. *Journal of the Occupational and Environmental Hygiene*, *9*(7), 443–449.

Liu, F., Qian, H., Luo, Z., & Zheng, X. (2021). The impact of indoor thermal stratification on the dispersion of human speech droplets. *Indoor Air*, *31*(2), 369–382.

Mofakham, A. A., Helenbrook, B. T., Erath, B. D., Ferro, A. R., Ahmed, T., Brown, D. M., et al. (2022). On the variation of fricative airflow dynamics with vocal tract geometry and speech loudness. *Aerosol Science and Technology*, *56*(5), 446–460.

Morsi, S., & Alexander, A. (1972). An investigation of particle trajectories in two-phase flow systems. *Journal of Fluid Mechanics*, *55*(2), 193–208.

Narayanan, S. S., Alwan, A. A., & Haker, K. (1995). An articulatory study of fricative consonants using magnetic resonance imaging. *The Journal of the Acoustical Society of America*, *98*(3), 1325–1347.

Narayanan, S., Toutios, A., Ramanarayanan, V., Lammert, A., Kim, J., Lee, S., et al. (2014). Real-time magnetic resonance imaging and electromagnetic articulography database for speech production research (TC). *The Journal of the Acoustical Society of America*, *136*(3), 1307–1311.

Oller, D. K. (1973). The effect of position in utterance on speech segment duration in English. *The Journal of the Acoustical Society of America*, *54*(5), 1235–1247.

Ounis, H., Ahmadi, G., & McLaughlin, J. B. (1991). Brownian diffusion of submicrometer particles in the viscous sublayer. *Journal of Colloid and Interface Science*, *143*(1), 266–277.

Pont, A., Guasch, O., Baiges, J., Codina, R., & Van Hirtum, A. (2019). Computational aeroacoustics to identify sound sources in the generation of sibilant/s. *International Journal for Numerical Methods in Biomedical Engineering*, *35*(1), Article e3153.

Singhal, R., Ravichandran, S., Govindarajan, R., & Diwan, S. S. (2021). Virus transmission by aerosol transport during short conversations. arXiv preprint arXiv:2103.16415.

Stadnytskyi, V., Bax, C. E., Bax, A., & Anfinrud, P. (2020). The airborne lifetime of small speech droplets and their potential importance in SARS-CoV-2 transmission. *Proceedings of the National Academy of Sciences*, *117*(22), 11875–11877.

Titze, I. R., & Martin, D. W. (1998). *Principles of voice production*. Acoustical Society of America.

Wang, J., & Li, Y. (2019). Research on children's mandarin Chinese voiceless consonant airflow [a]. In *2019 3rd international conference on art design, language and humanities (ADLH 2019)[C]* (pp. 210–216).

Yan, J., Grantham, M., Pantelic, J., De Mesquita, P. J. B., Albert, B., Liu, F., et al. (2018). Infectious virus in exhaled breath of symptomatic seasonal influenza cases from a college community. *Proceedings of the National Academy of Sciences*, *115*(5), 1081–1086.

Yang, F., Pahlavan, A. A., Mendez, S., Abkarian, M., & Stone, H. A. (2020). Towards improved social distancing guidelines: Space and time dependence of virus transmission from speech-driven aerosol transport between two individuals. *Physical Review Fluids*, *5*(12), Article 122501.

Yoshinaga, T., Nozaki, K., & Wada, S. (2019). A simplified vocal tract model for articulation of [s]: The effect of tongue tip elevation on [s]. *PLoS One*, *14*(10), Article e0223382.